ELSEVIER

Journal of Power Sources 92 (2001) 124–130

JOURNAL OF POWER SOURCES

www.elsevier.com/locate/jpowsour

Synthesis of $LiMn_2O_4$ powder by auto-ignited combustion of poly(acrylic acid)-metal nitrate precursor

Hyu-Bum Park[a,*], Jeongsoo Kim[b], Chi-Woo Lee[a,c]

[a]*Institute of Science and Technology, Korea University, Seochang-Ri, Chochiwon, Chungnam 339-700, South Korea*
[b]*Department of Materials Science and Engineering, University of Seoul, Jeonnong-dong, Tongdaemun-ku, Seoul 130-743, South Korea*
[c]*Division of Natural Sciences, College of Sciences and Technology, Korea University, Seochang-Ri, Chochiwon, Chungnam 339-700, South Korea*

Received 11 August 1999; received in revised form 21 January 2000; accepted 24 May 2000

Abstract

Spinel $LiMn_2O_4$ powder has been prepared by an auto-ignited combustion of poly(acrylic acid) (PAA)-metal nitrate precursor. The formation route to spinel $LiMn_2O_4$ phase from the precursor strongly depends on the mole ratio (MR) of PAA to metal nitrate. The precursors with MR=1.0 and 6.0 directly produced crystalline $LiMn_2O_4$ powders by the auto-ignited combustion at very low temperature (200°C), whereas the precursor with MR=3.0 produced Mn_3O_4, MnO, and carbonate at the auto-ignited combustion stage and formed spinel $LiMn_2O_4$ phase after further calcinations at higher temperatures. The obtained $LiMn_2O_4$ powders are composed of very fine primary particles (<100 nm) but highly agglomerates and have surface area of 14–29 $m^2\ g^{-1}$.

Keywords: $LiMn_2O_4$; Synthesis; PAA; Auto-ignited combustion

1. Introduction

Lithium transition metal oxides, spinel $LiMn_2O_4$ and layered $LiCoO_2$ and $LiNiO_2$, have been studied as cathode materials for Li-ion rechargeable batteries. For the past 10 years, the spinel $LiMn_2O_4$ has been studied extensively because of its economical and environmental advantages; Mn is abundant and significantly cheaper than Co and Ni, and $LiMn_2O_4$ is the least toxic among these compounds.

$LiMn_2O_4$ has been usually synthesized using solid-state reactions that involve the mechanical mixing of oxides and/or carbonates followed by high temperature firing and extended grinding. This method, which requires long-range diffusion of metal ions, may result in non-homogeneity, larger particles, and poor control of stoichiometry. Several solution methods using soluble metal ion sources have been used to synthesize mixed-cation oxide powders [1–6]. Among the solution methods, techniques based on using organic polymers as a gelling and/or complexing agent have been developed by several investigators. Recently, $LiMn_2O_4$ powders have been successfully synthesized through the formation of polymeric precursors [1–3]. For example, Liu et al. [1] have reported the synthesis and electrochemical studies of $LiMn_2O_4$ powders prepared by the Pechini process. Sun et al. [2] have prepared $LiMn_2O_4$ by a sol–gel method using an aqueous solution of metal acetates containing poly(acrylic acid) (PAA) as a chelating agent. Park et al. [3] also have prepared $LiMn_2O_4$ powders by an auto-ignited combustion of poly(ethylene glycol)-metal nitrate precursor.

In the present study, we report the synthesis of $LiMn_2O_4$ powder by an auto-ignited combustion of PAA-metal nitrate gel precursor at very low temperature. The formation route of $LiMn_2O_4$ from the precursor has been studied by X-ray diffraction (XRD) and infrared (IR) spectroscopy. In addition, powder characteristics were investigated by scanning electron microscopy (SEM), particle size analysis, and elemental analysis.

2. Experimental

Reagent-grade $LiNO_3$, $Mn(NO_3)_2{\times}H_2O$, and PAA solution were used as starting materials. In order to determine the content of Mn in $Mn(NO_3)_2{\times}H_2O$, a stock solution was prepared and standardized by EDTA titration. PAA-metal nitrate precursor was prepared as described below. At first, stoichiometric amounts of $LiNO_3$ (0.05 mol) and $Mn(NO_3)_2$ solution (0.10 mol) were dissolved in distilled water, and then PAA solution (0.05, 0.15, and 0.30 mol of repeating unit, –(CH(COOH)CH_2)–) was added to the mixed-metal ion solution. The mole ratio (MR) of PAA to $LiMn_2(NO_3)_5$

* Corresponding author. Tel.: +82-41-860-1919; fax: +82-41-865-7122.
E-mail address: parkhb@tiger.korea.ac.kr (H.-B. Park).

0378-7753/01/$ – see front matter
PII: S0378-7753(00)00512-7

is 1.0, 3.0, and 6.0. The mixed solution was heated at about 90°C for 1 day with stirring to evaporate excess water. As water evaporated, the solution became viscous and finally formed a very viscous gel precursor with pale brown color. The obtained gel precursor was placed in a furnace preheated to 200°C. After several minutes, the precursor automatically ignited and burnt with appearance of flame. This burnt powder was calcined further at 300, 500, and 700°C for 2 h.

Thermogravimetric analysis (TGA) and differential scanning calorimetry (DSC) of the gel precursors were performed at a heating rate of 20°C min^{-1} in static air with TGA-1000 and DSC-1500 instruments from Stanton Redcroft Co. XRD patterns of the burnt and the calcined powders were taken with a Rigaku D-Max III diffractometer using Cu Kα radiation to characterize crystalline phases. Lattice parameter was calculated by using eight XRD peaks and by applying a least square method. Crystallite size was calculated by using Scherrer's equation [7] and Si powder as a standard. FT-IR spectra of pellets pressed with KBr were measured using a Bomem MB-102 spectrometer. Elemental analysis was carried out by a Carlo–Erba EA1108 elemental analyser to determine residual amounts of elemental C, H, and N in the obtained powders. Average oxidation state of Mn was determined by the oxalate redox titration method [8]. To investigate the characteristics of powders, SEM micrographs were taken with a Hitachi S-4100 microscope and particle size distribution was measured by a Cilas–Alcatel HR850 granulometer in water. The specific surface area was measured by the Brunauer–Emmett–Teller (BET) method using N_2 gas with a Quantachrome Autosorb.

3. Results and discussion

In this study, PAA was used to enhance the homogeneous mixing of metal ions and to suppress the precipitation of metal nitrates during water evaporation. Since PAA has electronegative oxygen atoms, it can interact with electropositive metal ion [9]. This interaction and the random arrangement of polymer chain probably enhance homogeneous mixing of lithium and manganese metal ions on a molecular scale throughout polymeric matrix. Such a structure can eliminate the need for long-range diffusion during the formation of $LiMn_2O_4$. Therefore, at a relatively low temperature the precursor can form a homogeneous single phase of precise stoichiometry. Furthermore, PAA can serve as a fuel, being oxidized by the nitrate ions, and thus, cause auto-ignited self-propagating combustion of the precursor.

3.1. Thermal analysis of precursor

The pyrolysis of the dried gel precursors was investigated by DSC (Fig. 1) and TGA (Fig. 2). The DSC curves show endothermic peaks below 160°C accompanied by small weight losses, which correspond to evaporation of residual

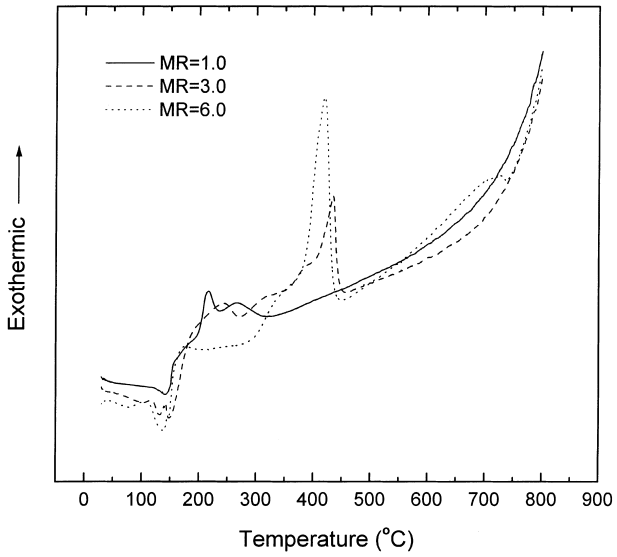

Fig. 1. DSC curves of the gel precursors with MR=1.0, 3.0, and 6.0, and pure PAA.

water. Above 160°C, the precursor with MR=1.0 shows broad exotherms between 170 and 320°C and the precursors with MR=3.0 and 6.0 extend exothermic region to higher temperatures. The total area of exothermic peak is related to the amount of PAA in the precursors. The strong exothermic peaks at 434°C for MR=3.0 and at 418°C for MR=6.0 accompanying with nearly no weight loss are possibly caused by the air combustion of carbonaceous materials formed from PAA. TGA curves show that the precursor with MR=1.0 gains and drastically loses weight at 205°C, whereas those with MR=3.0 and 6.0 show stepwise weight losses up to 450°C. The weight gain and drastic weight loss of MR=1.0 can be explained by an auto-ignited combustion.

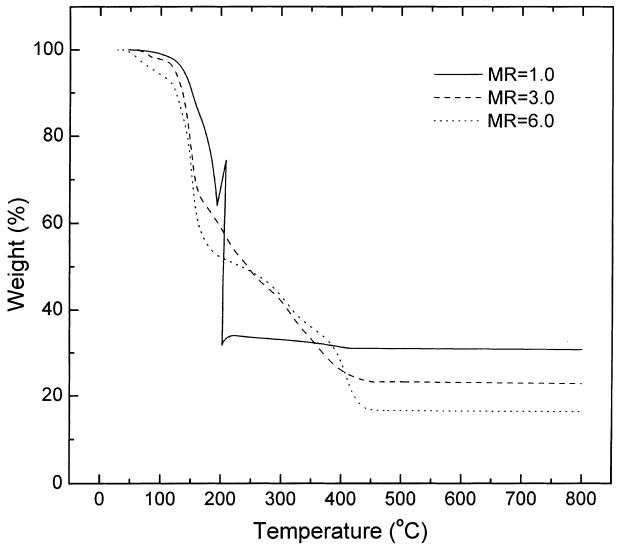

Fig. 2. TGA curves of the gel precursors with MR=1.0, 3.0, and 6.0, and pure PAA.

The precursor of MR=1.0 auto-ignited at 205°C and most of precursor burned out within very short time period with emitting heat and gases. The produced gases push down the sample container leading to weight gain. For all the precursors, the weight losses almost completed below 450°C. The total weight loss increases with the increase of MR depending on the amount of PAA and NO_3^- in the precursors. If the temperature of the reaction system increases to higher than 450°C by heat produced from the auto-ignited combustion of the precursors, it is expected that the precursors are decomposed to form metal oxide compounds, accompanying the weight losses due to decomposition of NO_3^- and PAA.

3.2. Burning behavior of precursor

The burning behavior of the dried gel precursors placed in an electric furnace preheated to 200°C was observed. After a few minutes, the precursor bloated and charred with giving out reddish brown gas (NO_2), and then the precursors automatically ignited and burned. The burning behavior was strongly dependent on MR related to the ratio of fuel (PAA) to oxidizer ($LiMn_2(NO_3)_5$). For MR=1.0, if the precursor once ignited at a part of bulk precursor, weak flame rapidly propagated through the bulk of precursor like a burning fuse and grey-black fluffy powder was obtained. For MR=3.0, the gel precursor burned most explosively with flame emitting bright red light and formed grey-brown powder, and the burning process completed in a few seconds. For MR=6.0, only faint dark-red light without flame intermittently propagated for several minutes, and grey-black powder was obtained.

These burning behaviors can be explained by introducing the concepts of propellant chemistry used by Park et al. [3,10]. According to the concepts, the metal nitrates and PAA can act as an oxidizing agent (oxidizer) and a reducing agent (fuel), respectively. Since the oxidizer coexists closely with the fuel in a homogeneously mixed state, a self-propagating redox reaction between the metal nitrates and PAA can readily occur. Therefore, PAA and nitrate ions burn out simultaneously to form metal oxides in very short time with raising the temperature of the reaction system. The reactivity is expected to depend on the ratio of oxidant to fuel, namely, MR. The most violent reaction of MR=3.0 implies that the most proper ratio of fuel to oxidizer is 3.0 for the PAA-$LiMn_2(NO_3)_5$ redox reaction system.

3.3. Formation route of $LiMn_2O_4$

XRD patterns (Fig. 3) were taken to investigate the formation of crystalline phases with increasing calcination temperature. For MR=1.0 and 6.0, the cubic spinel $LiMn_2O_4$ phase was formed directly by the auto-ignited combustion of the precursors even at very low temperature 200°C and maintained to calcination at 700°C. However, the XRD pattern of the burnt powder with MR=3.0 has MnO (manganosite), and Mn_3O_4 (hausmannite) phases, which disappear by calcination at 500°C. A small impurity peak possibly caused by Mn_2O_3 (bixbyite) coexisting with $LiMn_2O_4$ was observed even after calcination at 700°C. Fig. 4 shows the variation of cubic lattice parameter, a, for the burnt and calcined powder. The lattice parameter for MR=1.0 and 6.0 shows a minimum at 300°C and increases with increasing calcination temperature.

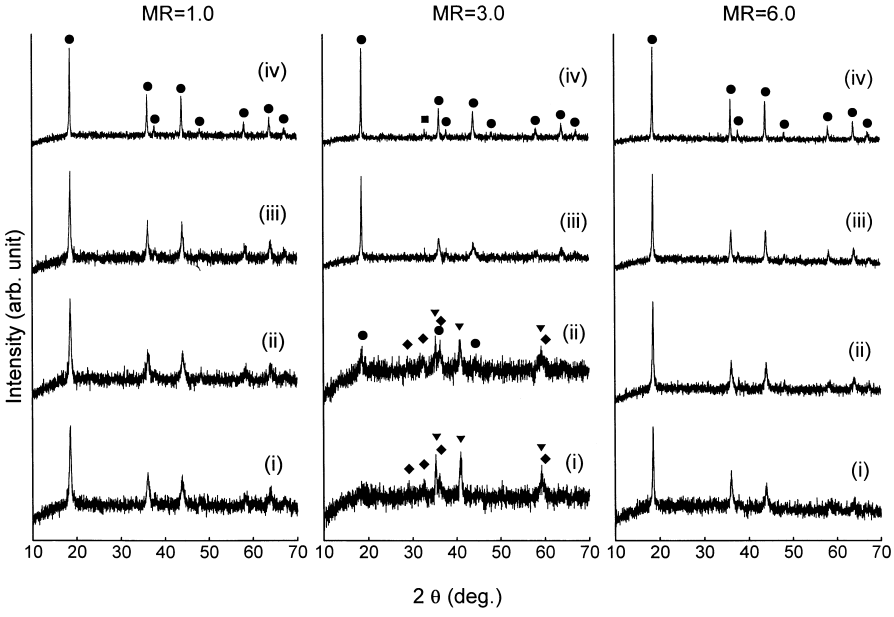

Fig. 3. XRD patterns of $LiMn_2O_4$ powder produced by burning and subsequent calcinations of the gel precursors with MR=1.0, 3.0, and 6.0: (i) burnt powder at 200°C; and calcined powders at (°C) (ii) 300; (iii) 500 and (iv) 700 for 2 h. (●): $LiMn_2O_4$; (▼): MnO (◆): Mn_3O_4; (■): Mn_2O_3.

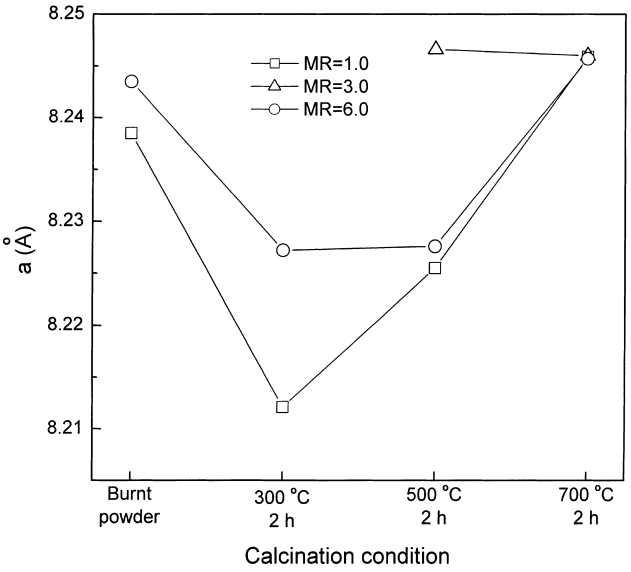

Fig. 4. Variation of lattice parameter, a, as a function of calcination temperature.

IR spectra are shown in Fig. 5. All the powders calcined at 700°C shows two bands at 610 and 510 cm^{-1}, which agree with those of $LiMn_2O_4$ reported by Wen et al. [11] and Endres et al. [12] (the bands observed at 3430 and 1628 cm^{-1} are due to water absorbed in KBr). The gel precursors show many complex bands corresponding to stretching and bending modes from PAA, metal nitrates, and residual water. The burnt powders show different spectra. For MR=1.0, a small characteristic peak of nitrate ion remained at 1385 cm^{-1} in addition to two bands of $LiMn_2O_4$ [10,13]. For MR=3.0, three peaks at 1497, 1436, and 864 cm^{-1} due to carbonate ion [14,15] and complex peaks possibly due to metal–oxygen bond below 750 cm^{-1} were observed and remained up to calcination at 300°C for 2 h. This carbonate can be formed by the reaction of Li (or Mn) ion with CO_2 gas evolved from the combustion of PAA. The carbonate may be amorphous type (or lithium carbonate having lower X-ray scattering power) because any detectable carbonate peaks were not observed in XRD pattern. For MR=6.0, the peaks of organic residue besides $LiMn_2O_4$ was observed, and two peaks at 1566 and 1429 cm^{-1} are very similar to those of metal-carboxylic acid complex, indicating that the acid group of PAA was not fully decomposed [13,15]. All the calcined powders for MR=6.0 show only two peaks of $LiMn_2O_4$.

Based on the XRD and IR results, a tentative $LiMn_2O_4$ formation path for MR=1.0, 3.0 and 6.0 including the possible intermediate phase formations may be proposed in Table 1. The formation route is highly dependent on the MR. Crystalline $LiMn_2O_4$ phase was obtained directly by the auto-ignited combustion of the gel precursors when the burning process is not violent, i.e. when MR=1.0 and 6.0. It is suggested that a mild reaction between fuel and oxidizer is necessary to produce $LiMn_2O_4$ phase at low temperature.

It has been well known that the oxidation state of Mn in oxide-type compounds is dependent on both temperature and partial pressure of oxygen, it decreases as the temperature increases and the partial pressure of oxygen decreases [16]. According to the phase diagram determined by using calorimetry, MnO_2 is stable below about 420°C, Mn_2O_3 between 420 and 730°C, Mn_3O_4 beyond 730°C, and MnO in

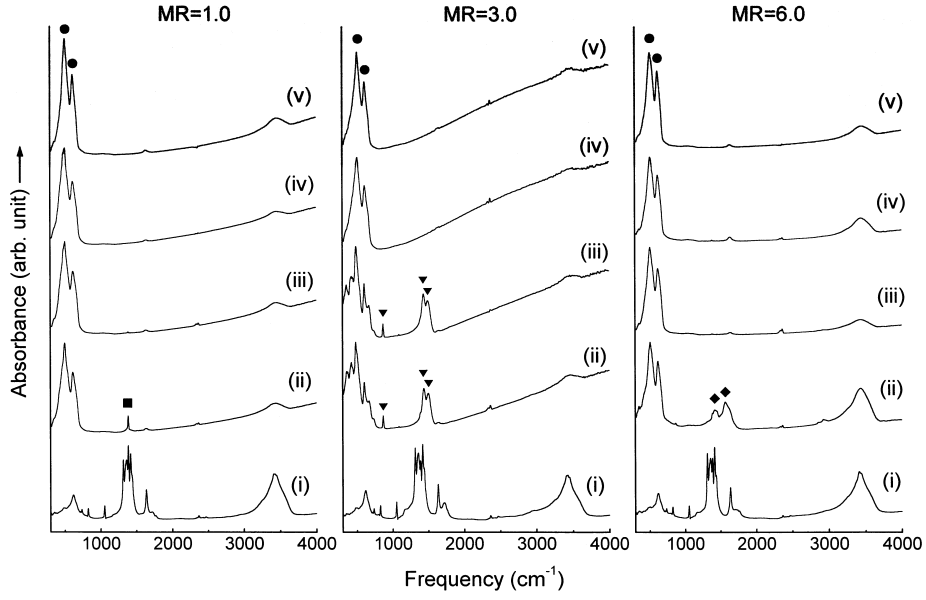

Fig. 5. IR spectra of $LiMn_2O_4$ powder produced by burning and subsequent calcinations of the gel precursors with MR=1.0,3.0, and 6.0: (i) precursor; (ii) burnt powder at 200°C; and calcined powders at (°C) (iii) 300; (iv) 500 and (v) 700 for 2 h. (●): $LiMn_2O_4$; (■): nitrate; (▼): carbonate; (◆): metal carboxylate.

Table 1
Formation route of spinel $LiMn_2O_4$ phase from the PAA-metal nitrate gel precursors

MR	Burning at 200°C	Calcination temperature (°C)		
		300	500	700
1.0	$LiMn_2O_4$+nitrate	$LiMn_2O_4$	$LiMn_2O_4$	$LiMn_2O_4$
3.0	MnO+Mn_3O_4+carbonate	MnO+Mn_3O_4+$LiMn_2O_4$+carbonate	$LiMn_2O_4$+Mn_2O_3(t)	$LiMn_2O_4$+Mn_2O_3(t)
6.0	$LiMn_2O_4$+organic residue	$LiMn_2O_4$	$LiMn_2O_4$	$LiMn_2O_4$

much higher temperature region in air. The burnt powder of MR=3.0 was composed of some Mn–O phases, such as MnO and Mn_3O_4 with lower oxidation states (+2 or +3) than $LiMn_2O_4$ (+3.5). MnO has been hardly found in other reports on the preparation of $LiMn_2O_4$. At the burning stage, the redox reaction of nitrate with PAA can produce the heat, which leads to the increase of temperature in the reaction system. Furthermore, CO gas having reducing power can be produced by an incomplete combustion of PAA. Consequently, the two factors can cooperatively suppress the oxidation of Mn^{2+} to Mn^{4+}, and thus, Mn–O compounds with lower oxidation states were formed during the burning process. If oxygen is supplied from air in sufficient quantity during the subsequent calcinations, the Mn–O oxides with lower oxidation states are transformed to the more stable $LiMn_2O_4$.

The variation of lattice parameter for MR=1.0 and 6.0, in which cubic spinel $LiMn_2O_4$ phase was prepared directly by the auto-ignited combustion, shows a minimum at 300°C and then increases with increased calcination temperature. In $LiMn_2O_{4+x}$ spinel system, the lattice parameter is well known to increase with the decrease of Mn oxidation state because of the difference of ionic radius between Mn^{3+} and Mn^{4+} [17–19]. The oxidation state of Mn was measured for the samples with MR=1.0, in which single spinel phases were formed and its burnt powder has least impurity (see Table 2). The measured Mn oxidation state of the burnt powder is +3.40 and that of the powders calcined at 300, 500 and 700°C is +3.57, +3.54 and +3.51, respectively. The unusual low Mn oxidation state (+3.4) of the burnt powder can be caused by combustion heat and reducing atmosphere, as described above. Thus, the large lattice parameter of the burnt powder was possibly resulted from the low Mn oxidation state. The large lattice parameter of the burnt powder decreases by air oxidation of Mn form +3.40 to +3.57 during calcination at 300°C for 2 h. In the calcined powder series, the increase of lattice parameter with calcination temperature is also believed to be due to the decrease of Mn oxidation state from +3.57 to +3.51 [17–19].

Table 2
Elemental analysis results of the burnt and the calcined powder (wt.%)

MR	Element	Burning at 200°C	Calcination temperature (°C)		
			300	500	700
1.0	C	0.23	0.14	0.11	0.03
	H	–[a]	–	–	–
	N	0.20	0.05	0.03	0.03
3.0	C	1.89	1.89	0.07	0.06
	H	–	–	–	–
	N	–	–	–	–
6.0	C	14.34	0.12	0.05	0.05
	H	0.73	–	–	–
	N	0.70	–	–	–

[a] Below detection limit.

3.4. Characterization of $LiMn_2O_4$ powder

Unlike in the solid state reaction, it is anticipated that some components of precursor, such as carbon, hydrogen, and nitrogen, can remain in $LiMn_2O_4$ powder prepared at low temperatures, especially, when an organic polymer is used as a gelling agent. In order to know how much carbon, hydrogen, and nitrogen exist in the obtained powders, elemental analysis was carried out. Results are illustrated in Table 2. The residual amount of elemental carbon for the burnt powders decreases with increasing calcination temperature and decreasing MR. The burnt powder of MR=6.0 contains hydrogen, indicating that organic residue from PAA remains. For MR=1.0 and 6.0, the residual carbon, hydrogen, and nitrogen was almost removed from the powders only by calcination at 300°C. In the case of MR=1.0, $LiMn_2O_4$ powder with very low impurities was formed directly by the auto-ignited burning of the precursors at 200°C.

Crystallite sizes calculated by Scherrer's equation [7] and specific surface areas measured by the BET method are listed in Table 3. The crystallite size ranges from 14 to 52 nm

Table 3
Crystallite size and BET surface area of the calcined $LiMn_2O_4$ powders

MR	Crystallite size (nm)			BET surface area ($m^2\ g^{-1}$)[a]
	300°C	500°C	700°C	
1.0	14	22	46	28.8
3.0			47	17.4
6.0	17	26	52	14.7

[a] For powders calcined at 700°C for 2 h.

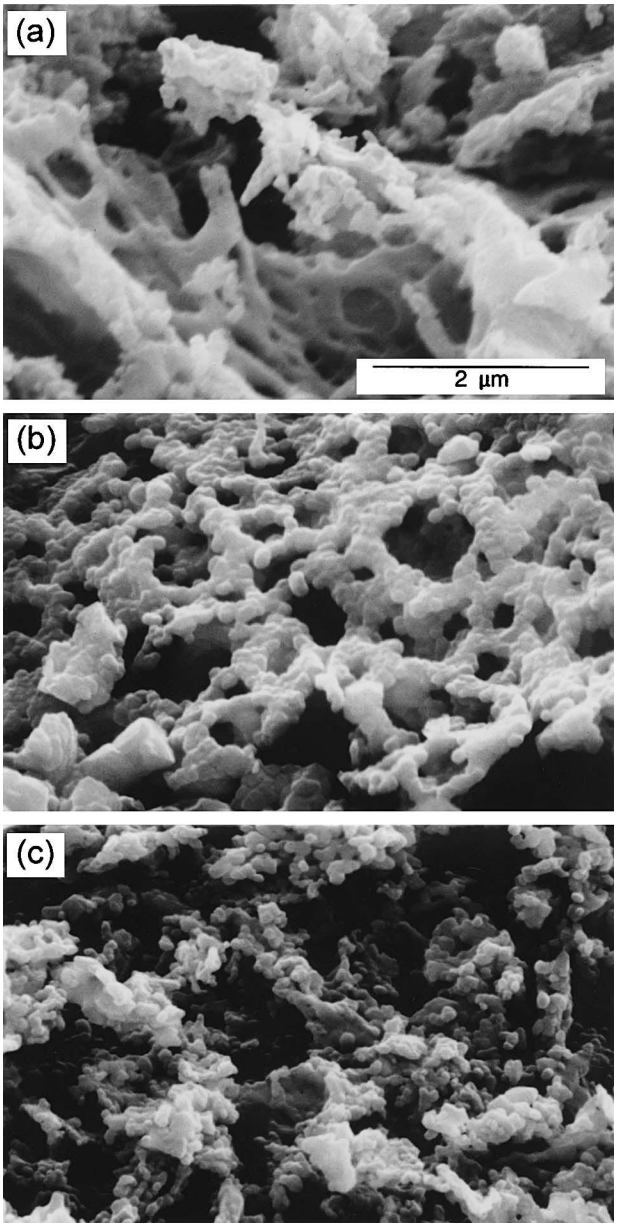

Fig. 6. SEM photographs of $LiMn_2O_4$ powders produced by calcinations of the gel precursors with MR: (a) 1.0; (b) 3.0 and (c) 6.0, at 700°C for 2 h.

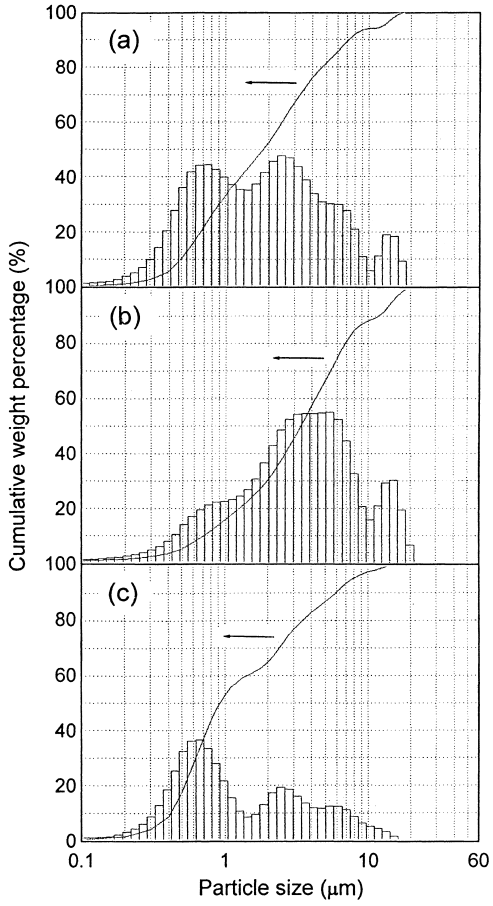

Fig. 7. Particle size distributions and cumulative weight percentage curves of $LiMn_2O_4$ powders produced by calcinations of the gel precursors with MR: (a) 1.0; (b) 3.0 and (c) 6.0, at 700°C for 2 h.

and increases with the increase of calcination temperature. The powders calcined at 700°C have specific surface area of 14–29 $m^2\ g^{-1}$. SEM photographs (Fig. 6) of $LiMn_2O_4$ powders calcined at 700°C for 2 h shows that the product consists of very fine primary particles (<100 nm) but highly agglomerates, containing pores presumably formed by gas evolution at the burning stage. Particle size analysis was performed to check the degree of agglomeration and the results are illustrated in Fig. 7. All the powders calcined at 700°C have broad particle size distributions and the content of particles smaller than 1 μm in diameter is 33% for MR=1.0, 16% for MR=3.0, and 53% for MR=6.0.

4. Conclusions

$LiMn_2O_4$ powder was synthesized successfully by the auto-ignited combustion of PAA-metal nitrate gel precursor. The burning behavior of the gel precursors strongly depended on the MR of PAA to metal nitrate. The spinel $LiMn_2O_4$ phase was synthesized only by the combustion of the precursor even at very low temperature 200°C for MR=1.0 and 6.0; particularly, the burnt powder with MR=1.0 has very small impurity. However, when MR=3.0, the combustion produced manganese oxides containing lower valent Mn ions and carbonate, which disappeared by subsequent calcination at 500°C. The formation of manganese oxides with lower valent Mn ions could be explained in terms of the heat and the reducing atmosphere produced by the reaction between oxidizer and fuel coexisting in the precursors. The obtained powders are composed of very fine primary particles (<100 nm) and have surface area of 14–29 $m^2\ g^{-1}$, but highly agglomerates and, thus, show broad particle size distributions.

References

[1] W. Liu, G.C. Farrington, F. Chaput, B. Dunn, J. Electrochem. Soc. 143 (1996) 879.
[2] Yang-Kook Sun, In-Hwan Oh, Kwang Yul Kim, Ind. Eng. Chem. Res. 36 (1997) 4839.
[3] Hyu-Bum Park, Young-Sik Hong, Ji-Eun Yi, Ho-Jin Kweon, Si-Joong Kim, Bull. Korean Chem. Soc. 18 (1997) 612.
[4] J.-H. Choy, D.-H. Kim, C.-W. Kwon, Y.-I. Kim, J. Power Sources 77 (1999) 1.
[5] Young-Sik Hong, Hyu-Bum Park, Ji-Eun Yi, Chi-Hwan Han, Si-Joong Kim, Bull. Korean Chem. Soc. 18 (1997) 1153.
[6] S.R.S. Prabaharan, M.S. Michael, T.P. Kumar, A. Mani, K. Athinarayanaswamy, R. Gangadharan, J. Mater. Chem. 5 (1995) 1035.
[7] B.D. Cullity, Elements of X-ray Diffraction, Addison-Wesley, Reading, MA, 1978, p. 284.
[8] A.I. Vogel, Vogel's Textbook of Quantitative Inorganic Analysis, 4th Edition, Longman, London, 1979, p. 356.
[9] H.H.J. Saniger, J. Garcia-Alejandre, V.M. Castano, Mater. Lett. 12 (1991) 281.
[10] Hyu-Bum Park, Ho-Jin Kweon, Young-Sik Hong, Si-Joong Kim, Keon Kim, J. Mater. Sci. 32 (1997) 57.
[11] S.J. Wen, T.J. Richardson, L. Ma, K.A. Striebel, P.N. Ross Jr., E.J. Cairns, J. Electrochem. Soc. 143 (1996) L136.
[12] P. Endres, B. Fuchs, S. Kemmler-Sack, K. Brandt, G. Faust-Becker, H.-W. Praas, Solid State Ionics 89 (1996) 221.
[13] H.-M. Zhang, Y. Teraoka, N. Yamazoe, Chem. Lett. 1987, p. 665.
[14] S.D. Ross, Inorganic Infrared and Raman Spectra, McGraw-Hill, London, UK, 1972.
[15] D. Hennings, W. Mayer, J. Solid State Chem. 26 (1978) 329.
[16] S. Fritsch, A. Navrotsky, J. Am. Ceram. Soc. 79 (1996) 1761.
[17] M. Hosoya, H. Ikuta, T. Uchida, M. Wakihara, J. Electrochem. Soc. 144 (1997) L52.
[18] C. Masquelier, M. Tabuchi, K. Ado, R. Kanno, Y. Kobayashi, Y. Maki, O. Nakamura, J.B. Goodenough, J. Solid State Chem. 123 (1996) 255.
[19] T. Takada, H. Enoki, H. Hayakawa, E. Akiba, J. Solid State Chem. 139 (1998) 290.